Soft Matter

Accepted Manuscript

ROYAL SOCIETY OF CHEMISTRY

www.rsc.org/softmatter

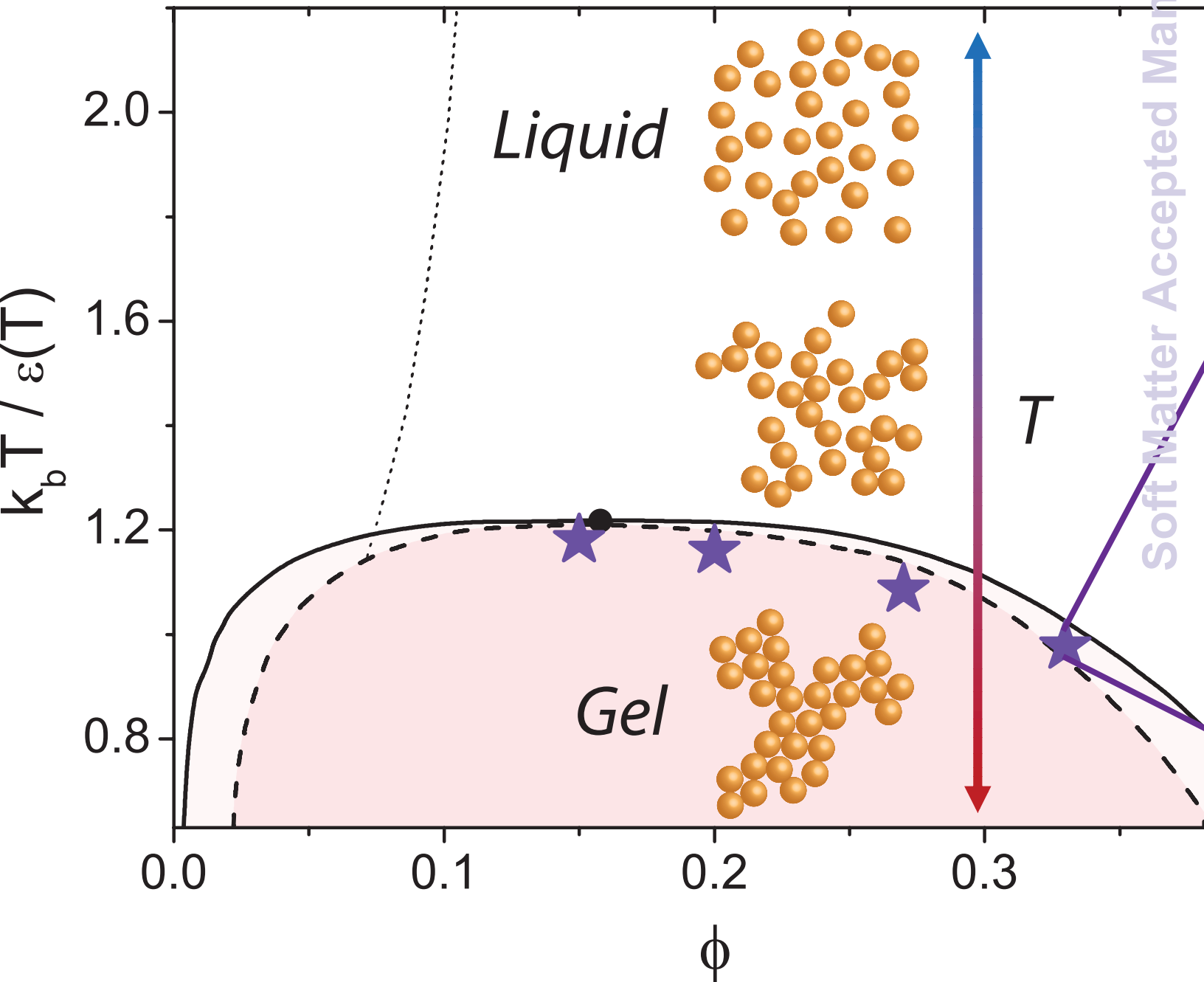

Soft Matter

RSCPublishing

ARTICLE

Microdynamics and arrest of coarsening during spinodal decomposition in thermoreversible colloidal gels†

Cite this: DOI: 10.1039/xoxxoooooox

Received 11th April 2015,
Accepted 13th June 2015

DOI: 10.1039/xoxxoooooox

www.rsc.org/

Yongxiang Gao[ab], Juntae Kim[a] and Matthew E. Helgeson*[a]

Coarsening and kinetic arrest of colloidal systems undergoing spinodal decomposition (SD) is a conserved motif for forming hierarchical, bicontinuous structures. Although the thermodynamic origins of SD in colloids are widely known, the microstructural processes responsible for its coarsening and associated dynamics *en route* to arrest remain elusive. To better elucidate the underlying large-scale microdynamical processes, we study a colloidal system with moderate-range attractions which displays characteristic features of arrested SD, and study its dynamics during coarsening through a combination of differential dynamic microscopy and real-space tracking. By extending recently developed imaging techniques, we reveal directly that the coarsening arises from collective dynamics of dense domains, which undergo slow, intermittent, and ballistic motion. These collective motions indicate interfacial effects to be the driving force of coarsening. The nature of the gelation enables to control the arrested length scale of coarsening by the depths of quenching into the spinodal regime, which we demonstrate to provide an effective means to control the elasticity of colloidal gels.

1 Introduction

Spinodal decomposition (SD) is a non-equilibrium de-mixing process whereby a homogeneous fluid spontaneously phase separates when quenched into the thermodynamically unstable coexistence region[1]. When it occurs, the system develops bicontinuous structure, with time-growing domains that are rich in one phase and poor in another.[2] In simple fluids, interfacial tension is sufficient to drive these domains to macroscopic scales, ultimately leading to complete phase separation. However, in systems where the kinetics in one or both phases are sufficiently quenched, SD can be effectively arrested, resulting in vitrification of the bi-continuous structure over observable time frames, with behavior that is qualitatively described by viscoelastic phase separation.[3] This phenomenon is ubiquitous in a wide range of systems including metal alloys,[4] polymer blends,[5] and the natural world.[6,7] In this way, arrested SD provides a generic route to produce biphasic materials.[8]

Colloidal gels are model systems for studying such arrested states,[9] and have long been hypothesized to form from arrested phase separation in certain systems.[10,11] Specifically, studies on dilute attractive colloids found gels comprised of sample-spanning networks with interpenetrating particle clusters and large voids.[12-14] This structure was proposed to result from interruption of phase separation of the colloid by an attractive glass transition which intersects the colloid-rich side of the vapour-liquid binodal,[14,15] as supported by computer simulations.[16] Such colloidal gels inherently have two distinct length scales: one corresponding to separations of nearest neighbour particles (manifest in enhanced short-range pair correlations), and the other corresponding to correlations between phase separated domains (signified by a low-q peak in the interparticle structure factor). In these cases, colloidal gelation is accompanied with a dramatic slowing down of the structural dynamics and emergence of solid-like mechanical properties.[17,18]

The influence of SD on gelation appears to be highly sensitive to the range of interparticle attraction, λ, relative to the particle diameter, σ. For colloids with short-range attractions ($\lambda/\sigma < 0.1$), the Noro-Frenkel law of corresponding states is found to apply, where computer simulations and theoretical calculations show that the boundaries at which SD occurs are essentially independent of the shape and range of attraction.[19,20] Under these conditions, the gelation boundary identified experimentally by Lu *et al.*[14] compares well with the fluid-fluid binodal predicted from theory. Systems with moderate-range attractions ($0.1 < \lambda/\sigma < 0.3$) exhibit phase coexistence boundaries that depend significantly on the range of the potential.[21] Nevertheless, gelation in experimental systems with moderate-range attraction can also occur close to the fluid-fluid spinodal,[12,20] suggesting that gelation proceeds by kinetic arrest of phase instability.[12,22] Finally, for longer-range attractions ($\lambda/\sigma > 0.3$), the colloidal fluid can undergo complete coarsening to a nearly macroscopic phase separated state,[23] depending on the depth of quenching into the spinodal regime,[24,25] as also suggested by simulations.[26] It has therefore been hypothesized that for intermediate and long-range

attractions, the system processes through the homogeneous fluid phase, followed by phase separation that eventually arrests as the system is progressively quenched.[25]

Although the fully arrested states of phase separating gels have been well-studied, the microstructural processes that drive coarsening *en route* to gelation and arrest remain unclear. The reasons for this appear to be two-fold. First, there are relatively few experimental colloidal systems in which well-controlled quenches into the region of phase instability can be obtained, since most of the systems in which arrested phase separation is observed (i.e. depletion-induced gels) occur by mixing. Although colloids with thermoreversible attractions, such as alkane-grafted silica[27] or microemulsion-telechelic polymer mixtures,[28-30] potentially achieve such control, arrested phase separation has yet to be observed in these systems.

A second challenge is the multi-scale nature of dynamics in phase separating colloids. As previously mentioned, coarsening gels exhibit complex dynamics on two disparate length scales – the particle length scale, in which single colloids explore a complicated energy landscape in the dense domains, and the length scale of the phase separation, where interfacial- and viscoelasticity-driven motion play a significant role. So far, most microdynamic studies of arrested phase separation and gelation in colloidal systems have probed the former, smaller length scale (Fig. S1).[12,14,22,24,25,31-35] Essentially, these studies probe dynamics of particles within dense clusters comprising the colloid-rich domains. By localizing and tracking the motion of single micron-sized particles with time, video confocal microscopy[14,32,33,35] has directly revealed and provided insight into the heterogeneous short-time dynamics in these clusters.

Although previous studies characterized the growth kinetics of the characteristic scale of phase separation,[14,23,25] relatively few studies have been carried out to understand the micro-dynamic processes underlying them at these large length scales. So far, most studies have used scattering methods on gels in the fully arrested state, which revealed emergent anomalous dynamics whose source is still uncertain. Specifically, the intermediate scattering function (ISF) of systems spanning a wide range of volume fractions decays faster than expected for diffusive processes, best described by a compressed exponential functional, $f(q,t)\sim exp(-(t/\tau)^{\beta})$ with $\beta>1$, indicating superdiffusive dynamics.[31,36-38] The slow relaxation time was found to scale with wave vector as $\tau \sim q^{-1}$, suggesting ballistic-like motion, as confirmed by simulations.[39,40]

A phenomenological model based on the concept of "micro-collapse" events[41] was constructed to capture this behavior, which predicts $\beta = 1.5$.[36] However, the model fails to predict the later-observed q-dependence of β, and so it was extended to include phenomenologically "intermittent" events.[37] It has since been speculated that these complex dynamics may arise from collective motion of large particle clusters.[31] However, no study has been performed at such large length scales except in the very dilute limit (volume fraction, $\phi < 0.001$) (Fig. S1),[36,37] leaving the origin of these dynamics in question, particularly for concentrated systems. We stress that the previous measurements were on fully arrested systems, and it is unclear whether superdiffusive dynamics are also evident (and if so, what role they play) in coarsening of gels *en route* to arrest.

To address these challenges in understanding the coarsening and arrest of spinodal decomposition in colloidal systems, we have developed and studied an experimental system capable of well-controlled, thermoreversible quenching into the region of phase instability.[42-44] The system consists of oil-in-water nanoemulsion droplets in the presence of thermoresponsive end-functionalized polymers. The attractions between droplets in the system can be finely-tuned with temperature, resulting in colloidal gelation at elevated temperatures.[43] Recently, microstructural studies in the arrested state were used to hypothesize that gelation in the system could either occur by homogeneous percolation or arrested phase separation depending on the volume fraction ϕ under slow, quasi-equilibrium quenching.[42] In the latter case, it was found that the microstructure was best-described as an arrested bicontinuous network of a dense fractal-like phase and an unstructured dilute phase, whose long-range correlations were consistent with arrested phase separation. This finding differentiates these materials from the aforementioned microemulsion-telechelic mixtures, since they do not appear to exhibit arrested phase separation over any previously studied conditions.[28-30]

To better probe the microstructural processes controlling coarsening and arrest in phase separating colloidal gels, the present work seeks to elucidate the dynamics of SD in the nanoemulsion system *en route* to kinetic arrest and gelation at the relevant characteristic length scales of phase separation. In particular, we focus on shallow, quasi-equilibrium quenches at volume fractions above the critical point, $\phi > \phi_c$, for which relatively few experimental studies of microdynamics have been reported (Fig. S1).[22,31,33,35] Using thermosensitive nanoemulsions as a model system,[42-44] we apply recently developed techniques based on optical microscopy, including texture analysis microscopy (TAM)[45] and differential dynamic microscopy (DDM),[46,47] to probe the structural evolution of the system and confirm arrested spinodal decomposition as the mechanism of coarsening accompanying gelation. These techniques allow us to directly measure the evolution of large-scale fluid microstructure leading up to kinetic arrest, including the wave vector (q)-dependent dynamics encompassing the correlation length of the bicontinuous structure. We further track the net motion of individual droplet-rich domains, providing unprecedented insight into the nature and origin of anomalous dynamics during coarsening of colloidal gels. Finally, we examine how the arrested structure depends on the quench into the spinodal region, and compare it to the mechanical properties of the incipient gel.

2 Materials and methods

The material to be primarily studied in this work is an oil-in-water nanoemulsion containing a volume fraction, $\phi = 0.33$ of silicone oil droplets (kinematic viscosity = 5 cSt, density = 0.913 g/ml) with 200 mM sodium dodecyl sulphate (SDS) surfactant and 33 vol% poly(ethylene glycol diacrylate) polymer (PEGDA, 700 g mol^{-1}) in the aqueous phase (deionized water, 18.2 MΩ). As previously described,[43] the nanoemulsion was prepared using high-pressure homogenization (Avestin Emulsiflex-C5) for 20 passes at 10 kpsi, resulting in an average droplet radius a = 21 nm and PDI of 0.08, as measured by dynamic light scattering (DLS). The gravitational Peclet number[48] of the system is $Pe_g = 4\pi\Delta\rho g a^4/3k_BT \sim 2\times10^{-7}$, approximately 5 orders of magnitude smaller than the critical value (Pe_g^{crit}~0.01) beyond which gravity is shown to play a role in gelation.[49] We therefore do not expect sedimentation effects to play a significant role in our measurements. This assumption will be further tested in the experiments to follow. Further, we expect qualitatively different behaviour than larger emulsions where the kinetics of gelation are convoluted with sedimentation effects.[24,25] The sample was stored at 7 °C to slow Ostwald ripening.[43]

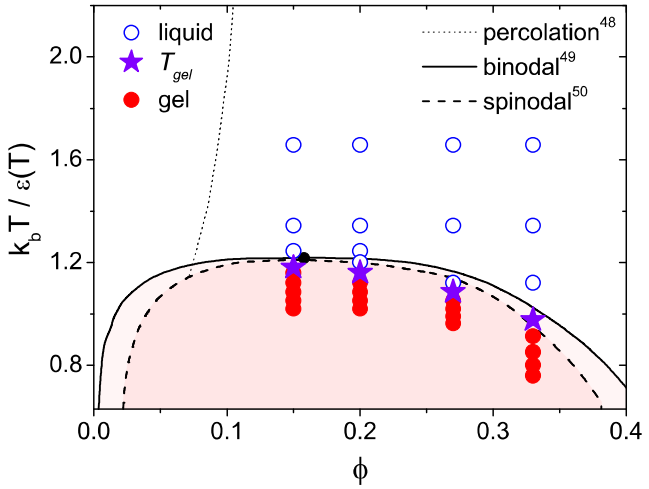

Fig. 1 Hypothetical phase diagram for the nanoemulsion system in this work. Lines indicate theoretical predictions[50-52] for the square well fluid with well depth ε and width $\lambda = 0.5\sigma$. Points correspond to the experimental state points studied in this work as determined by their rheology. Colloidal phases are identified by the rheology and light scattering measurements in Fig. 2.

The sample exhibits interdroplet attractions and colloidal gelation at elevated temperatures, which are believed to be due to interdroplet bridging of the polymer through partitioning of the hydrophobic PEG end groups at the oil-water interface.[43,44] The temperature dependence of the dilute pair potential was previously measured using small angle neutron scattering.[43] To summarize, the dilute structure factor is quantitatively described using a square well potential with fixed well width λ and temperature-dependent well depth, ε. Over the measureable temperature range, the well width is best fit by $\lambda = 0.47\sigma$ and its depth increases from ε/k_bT = 0.4 to 1.5 as the temperature is increased from 25 °C to 60 °C. It is important to note that a square well potential is unlikely to precisely capture the shape of the true potential due to polymer bridging.[53] Thus, the square well is only used here to facilitate qualitative comparison to theoretically predicted phase behavior (Fig. 1).[50-52]

The influence of polymer bridging as the source of interdroplet attractions in our nanoemulsion system bears resemblance to the telechelic polymer-microemulsion mixtures studied, for example, by Porte and co-workers.[28-30,54] However, we note an important qualitative difference – the fact that the present nanoemulsions exhibit gelation due to arrested phase separation at moderate ϕ, whereas in the microemulsions gelation only occurs in the homogeneous fluid phase, and macroscopic phase separation occurs in the region of phase instability. We believe this difference to be related to large quantitative differences in two important parameters – the number of adsorbing polymer ends per droplet, r, and the adsorption energy of a polymer end, E_a. For our nanoemulsions $r \sim O(10^3)$ whereas the microemulsions were limited to $r \sim O(10)$ before inducing macroscopic phase instability.[28] Furthermore, the telechelic polymers used for the microemulsion systems had relatively long hydrophobes, resulting in $E_a \sim O(12\text{-}18k_bT)$, whereas similar estimations for the present aqueous PEGDA polymers result in $E_a \sim O(2\text{-}3k_bT)$.[30] This is why, in the present system, the interdroplet attractions can be sensitively tuned with temperature, providing a means to accurately control the kinetic quench into the region of arrested phase instability.

We also note that the fluid nature of the droplets has been determined to have negligible effects on the colloidal behavior of these nanoemulsions.[42,43,55] Specifically, droplet deformability has no measurable influence for small droplet sizes,[44,45] nor does droplet instability impact the colloidal behaviour[44,45] since polymer bridging potentials typically possess a steep repulsive barrier at small separations,[53] causing aggregation of nanodroplets within a secondary minimum.

To probe gelation and coarsening in the sample, we combine measurements of the mechanical properties, structure and dynamics of the system. Due to the sensitive temperature-dependence of the system, extreme care was taken to control and monitor the sample temperature in each set of measurements to high precision. Rheological measurements were made on a stress controlled rheometer (AR-G2, TA instruments) with an upper-cone geometry (60 mm and 2°) and a Peltier temperature-controlled lower plate (±0.1 °C precision). DLS was measured on a multi-angle detector system (Brookhaven Instruments BI-200SM) equipped with a 637 nm (HeNe continuous wave) laser and a circulating temperature-control water bath (±0.5 °C precision), with measurements made at a fixed angle of 90° (q = 19.25 μm^{-1}). For optical microscopy, samples were loaded into home-built glass chambers with an inner height of 1 mm to avoid confinement effects, which are taped onto a dual Peltier-controlled thermal microscope stage (INSTEC, TSA02i, ±0.1 °C precision) to ensure good thermal contact. To minimize temperature gradients, the objective lens was warmed with a resistive temperature controller (Warner TC-124, Warner Instruments, ±1 °C precision). The temperature of the sample is monitored *in situ* with a thermocouple whose lead is attached to the top of the sample chamber. Due to the relatively low precision for temperature control of the objective, combined with its large thermal mass and temperature fluctuations in the surrounding air we observed occasional excursions in the sample temperature of up to ±0.5 °C over the course of some measurements. Cases where such excursions were evident will be explicitly mentioned in the results to follow. We directly image the fluid during gelation with an inverted optical microscope (Olympus IX71), equipped with a 40X objective lens (NA=0.75) and an Andor Clara digital camera (Andor Technology).

3 Results and discussion

3.1 Linear viscoelasticity

To identify the fluid-gel transition in the nanoemulsion system, we performed small amplitude oscillatory rheometry during gelation and aging under well-controlled temperature jumps. The results at several volume fractions are summarized in Figs. 1 and 2. Specifically, the incipient gelation temperature, T_{gel}, was identified as being where G' first crosses G'' and dominates the rheological behaviour (see Fig. S3).

To place the experimental nanoemulsion system on a colloidal phase diagram, we first interpolate the temperature-dependent well depth data in previous work[43] to an empirical sigmoidal relation (Fig. S2),

$$\varepsilon(T)/k_bT = \frac{a}{1+be^{-cT}} \qquad (1)$$

with resulting best-fit parameters (for T in °C) of a = 1.72±0.31, b = 10.4±4.3 and c = 0.069±0.021. We note that such a sigmoidal temperature-dependence has been predicted for other polymer-induced attractions, such as those arising between colloids with temperature-responsive polymer brushes.[56]

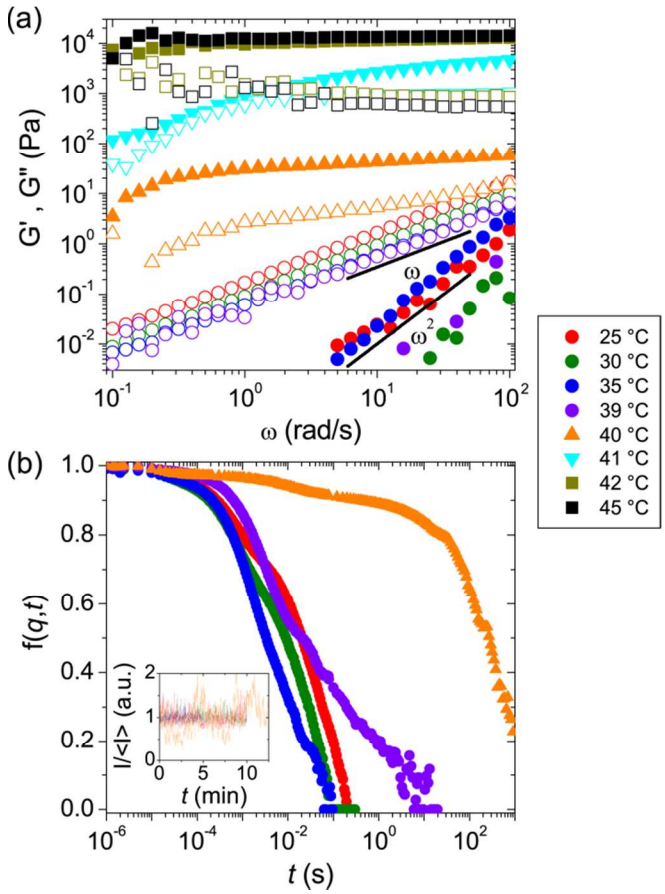

Fig. 2 Gelation of a temperature-responsive nanoemulsion with $\phi = 0.33$. (a) Temperature-dependent linear viscoelasticity of the nanoemulsion with $\phi = 0.33$. (b) Temperature-dependent ISF probed by DLS for q = 19.25 μm^{-1}. The signal is non-ergodic above 39 °C. Inset shows the time-dependent normalized intensity, with time re-scaled by a factor of 10 for the orange line to aid comparison.

From this relationship, we define an effective temperature for the system, $k_bT/\varepsilon(T)$, that should capture the phase behavior of the system, as well as the tendency for gel formation,[57] We note that, due to the temperature-dependence of the well depth (eq. 1), this effective temperature actually decreases with increasing experimental temperature. Fig. 1 shows state points determined from the rheological measurements on various volume fractions including liquid (open circles) and gels (closed circles), including the highest effective temperature (lowest experimental temperature) at which gelation is first observed, $k_bT_{gel}/\varepsilon(T_{gel})$,

It may seem counterintuitive that, in all cases, the gel point falls at temperatures where $\varepsilon(T_{gel})/k_bT_{gel} < 1$. We believe this is due to both the pathological nature as well as the long effective range of the square well potential. To better compare this result with other systems, we appeal to the Noro-Frenkel extended law of corresponding states,[20] which posits that potentials with varying shape but similar range can be quantitatively compared through the reduced second virial coefficient, $B_2^* = B_2/B_2^{HS}$, where B_2^{HS} is the hard-sphere value of the virial coefficient. For $\phi = 0.33$, we find $B_2^*(T_{gel}) = -2.74$. To compare this value with other gelling systems, we compare to the Asakura-Oosawa potential for polymer depletion attractions with various attraction range,[58,59] and find that this value of B_2^* is equivalent to attractions at contact of 3.4 k_bT and 2.4 k_bT for depletion potentials with maximum ranges of 0.25σ and 0.5σ, respectively. These strengths of attraction at the point of gelation compare favorably with those found experimentally for depletion systems with moderate-range attractions.[12]

Along with experimental data, Figure 1 also shows theoretical predictions of equilibrium colloidal phase behavior for the square well fluid with $\lambda = 0.5\sigma$.[50-52] Specifically, we compare to predictions of vapor-liquid equilibrium for the binodal from Gibbs ensemble Monte Carlo simulations[51] and the spinodal from integral equation theory,[52] as well as the percolation threshold as inferred from the pair connectedness function.[50] We find that the incipient gel point, k_bT_{gel}/ε identified by rheology is in fair agreement with the spinodal temperature predicted by theory. This suggests that gelation under these conditions coincides with spinodal decomposition, a hypothesis that will be tested by the experiments to follow.

The remainder of the experiments focused on $\phi = 0.33$, a sample in the dense regime that is well above the critical point ($\phi_c \sim 0.16$). We first probe the thermal rheology of the colloidal fluid by small amplitude oscillatory shear rheometry, and its dynamics by DLS at q = 19.25 μm^{-1} (Fig. 2). At temperatures below T_{gel}, we observe Newtonian behavior where G" ~ ω. The system is also ergodic for $T < T_{gel}$, i.e., $f(q,t)$ decays to zero over the experimental time window. When the temperature is increased above T_{gel}, G' and G'' increase significantly and become nearly independent of frequency, indicating solid-like behavior. Previous measurements found that at T_{gel}, critical scaling of the frequency-dependent moduli prove that the solid-like viscoelasticity is a result of gelation.[60] From this, we surmise that T_{gel} lies somewhere between 39-40 °C. Simultaneously, the system becomes non-ergodic, as shown in the slow dynamics in $f(q,t)$ and intermittent spikes in the raw count data during DLS measurements. We note that this non-ergodic behavior, in addition to multiple scattering, make it rather difficult to probe dynamics reliably with DLS once the system is quenched into the gel state. As such, the ISF above T_{gel} is only shown to distinguish it qualitatively from those below T_{gel}, as quantitative analysis of the dynamics is unreasonable under such conditions.[61]

3.2 Coarsening kinetics and microdynamics

To gain insight into the structural and dynamical behaviour of the system, we directly image the structural evolution of the sample using bright-field optical microscopy during gelation (Video S1). When T_{gel} is surpassed, the system develops observable heterogeneity, with alternating bright and dark regions, whose features evolve over time, slow down and eventually come to an arrested state (Fig. 3a). We note that, due to the shortcomings of the temperature control system, a small, <1 °C temperature increase of the sample was observed after the sample had come to arrest. According to eq. 1, this produces a change in the quench depth of $\Delta\varepsilon/k_bT < 0.029$, which is well below experimental uncertainty of the well depth and appeared to have no discernible effect on the arrested state (Fig. 3c). Nevertheless, in the dynamical measurements to follow, only data before this temperature increase was further analysed.

We surmise that the light and dark regions correspond to a coarsening phase separated structure of interlaced colloid-rich and colloid-lean domains. Such structure in this sample was suggested previously by neutron scattering and cryo-TEM measurements.[42,43] As the domains reach the micron-scale, they become directly visible under the microscope, and grow with increasing aging time, t_{age}, defined as the time elapsed after the sample reaches T_{gel}. We find that the bicontinuous structure can

be easily resolved by the imaging optics after t_{age} ~ 4 minutes. We further note that these domains appear at a length scale of microns, corresponding to hundreds of particle diameters, such that the detail of individual particles is not resolved.

The structural evolution is reminiscent of spinodal decomposition, whereby the correlation length of colloid-rich domains, L_c, coarsens over time. The fast Fourier transform (FFT) of the image is often used to extract L_c from optical images, where L_c can be inferred from the peak position of the radially-averaged power spectrum[45] as $L_c = 2\pi/q_{max}$, where q_{max} is the wavelength of maximum intensity, I_{max}. Here, we do not observe a clear peak in the FFT of the raw images due to image noise (Fig. S4). To obtain L_c, we instead employ a recently devised image analysis technique, texture analysis microscopy (TAM), the details of which are described elsewhere.[45] Briefly, TAM identifies a Gaussian kernel that best resembles the textural features in the raw image (in this case caused by the colloid-rich domains), which is used to construct a correlogram representing the probability density of finding an average textural feature at any location in the image (Video S2).

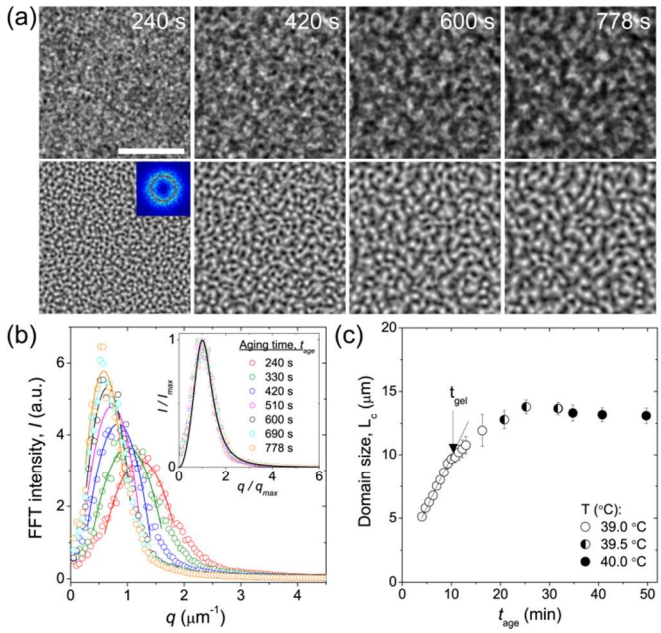

Fig. 3 Coarsening and arrest of spinodal decomposition in a colloidal fluid. (a) Time sequence of bright-field images (top) and resulting correlograms from TAM (bottom) for a coarsening nanoemulsion at T_{gel} = 39 °C. Scale bar represents 50 μm for all images. Inset is a Fourier transform of the correlogram. (b) Radially-averaged Fourier transforms of correlograms at the aging times indicated. The distributions are locally fit with a parabola (solid lines) to extract the peak position, q_{max}. Inset shows collapse of the curves by scaling q/q_{max} and I/I_{max}. Solid line shows predictions based on a theory for off-critical demixing.[62] (c) Coarsening kinetics of the characteristic length scale, $L_c = 2\pi/q_{max}$. Initially, L_c grows linearly (black line), with a rate of 12.8±0.6 nm/s. The time for the system to form a gel from rheological measurement (t_{gel}, G'=G'') is also indicated.

The results of this analysis are shown in Fig. 3a (bottom row). Best-fit TAM parameters can be found in Table S1. We then apply the FFT to the correlation maps to assess the average structural correlations (Fig. 3a, inset) through the radially-averaged FFT (Fig. 3b). In this case, we find a clear intensity peak, reminiscent of those obtained from confocal microscopy images.[14,63] In previous work, we showed that the location of the peak is not significantly influenced by the TAM process for images of sufficient contrast above background.[45] The data are fit locally with a parabolic function to extract q_{max} and I_{max}. Remarkably, we find that all the data collapse onto a single master curve by rescaling the data with q_{max} and I_{max} (Fig. 3b, inset). The master curve is well-described by a theoretical prediction for de-mixing due to off-critical fluctuations:[62]

$$I/I_{max} = \frac{3(q/q_{max})^2}{2+(q/q_{max})^6}. \qquad (2)$$

These results provide undisputable direct evidence that gelation in this system proceeds as arrested SD. Specifically, the structure evolves self-similarly over time with a single characteristic length scale, $L_c(t)$. At short aging times after the bi-continuous texture is observable by our microscope (~4 minutes), we find that L_c grows linearly with time (Fig. 3c), a hallmark of late-stage SD where evolution of the structure is dominated by interfacial coarsening.[2] After some time, the growth of L_c slows down, until it eventually saturates at a constant value, where it remains for a period of hours. We note that the aging time at which the growth of L_c slows coincides closely with the gel time (t_{gel}) at which solid-like rheology (G' > G") is first observed in kinetic rheology measurements (Fig. S3.2). This may suggest that network elasticity could play a significant role in the arrest of structural coarsening.

The observed growth kinetics differ from measurements of the coarsening of larger colloids under gravity, which exhibits power-law growth at long times.[24] This could be due to (1) the limited time scale accessed (t_{age} ~ 10^4-10^6 τ_B, where τ_B is the Brownian relaxation time) due to the influence of gravitational sedimentation, which is over an order of magnitude shorter than our study here; (2) much deeper quenches into the spinodal regime, whose effect on the growth of L_c is predicted by computer simulations[26] and suggested by viscoelastic phase separation;[3] or (3), the significant differences in volume fraction between the present study and this previous work (0.33 and 0.20, respectively). We note that earlier kinetic stages of SD where the coarsening is non-linear[2,23] are not observed here since L_c lies below the optical resolution at early age times.

To investigate the microstructural dynamics during coarsening we employ differential dynamic microscopy (DDM), a recently developed image analysis technique that gives information equivalent to multi-speckle scattering methods,[46,47] but is not as susceptible to multiple scattering and thus compatible with dense and opaque samples.[64] Briefly, the difference of two images separated by a lag time τ (Fig. 4a, first and second panels) is computed, resulting in a difference image (third panel). A magnified view of these images (Fig. S5) shows that DDM can detect intensity fluctuation, arising from structural reorganization, on length scales much smaller than the domain size. The FFT of the difference image is computed (fourth panel), and its power spectrum ($\Delta\bar{I}(q, \tau)^2$) is ensemble-averaged over all difference images at the same lag time τ. The average is performed over at least 100 images to ensure adequate statistics. Using this, we construct power spectra for all different lag time τ (Fig. 4b inset). The result is the dynamic structure function, $S(q,\tau)=<\Delta\bar{I}(q, \tau)^2>$, where $\bar{}$ and < > denote Fourier transform and ensemble average, respectively. $S(q,\tau)$ can be directly linked to the ISF measured by DLS when it is presented as a function of τ at various fixed q (Fig. 4b).

DDM has been applied to dispersed colloidal systems,[46,65,66] bacteria suspensions[64,67] and aggregation phenomena in dilute colloidal suspensions.[65,68] Here, we apply it for the first time to a dense colloidal system in which the structural elements are not individual particles, but rather dense fluid domains. This

allows us to extract microdynamics at large length scales (equivalent to hundreds of particle radii) encompassing the characteristic length scale, L_c. DDM was performed on the video microscopy images at three aging times: 4, 7, and 10 minutes. These aging times span the linear stage of coarsening to the onset of slowed growth. The results for $S(q,t)$ are well-described by the convolution of a short-time exponential decay and long-time anomalous dynamics (Fig. 4b),

$$S(q,\tau) = A(q)\left[1 - a(q)exp\left(-\left(\frac{\tau}{\tau_1(q)}\right)\right) - \left(1 - a(q)\right)exp\left(-\left(\frac{\tau}{\tau_2(q)}\right)^{\beta(q)}\right)\right] + B \qquad (3)$$

where $A(q)$ is an amplitude factor due to the static scattering of objects, a(q) is a coefficient ranging from 0-1 that expresses the proportion of the relaxation contributed by the exponential mode, and B is a q-independent contribution from incoherent background noise. The results for the ISF (the bracketed term) are shown in Fig. S6. The relaxation time of the fast mode scales as $\tau_1 \sim q^{-2}$ before flattening at low q, likely due to uncertainty in the fit for the fast mode since its contribution to the relaxation of $S(q,t)$ becomes vanishingly small at low q (Figs. 4c and S6, inset). The observation of $\tau_1 \sim q^{-2}$ is typical of diffusive behavior. It was previously shown that diffusive-like behavior in colloidal gels can arise from overdamped fluctuations of the collective motions within clusters.[69] We note that the relaxation times, τ_1, of the fast mode are of order 10^4-10^5 τ_B, which is similar to what was found in experiments confirming the presence of overdamped dynamics.[69] We therefore hypothesize that the short-time dynamics arise from thermal fluctuations of the cluster structure within individual dense domains.

By contrast, the relaxation time of the slow mode scales as $\tau_2 \sim q^{-1}$ (Fig. 4c), indicating ballistic-like dynamics.[39] Furthermore, we find that the slow mode decays faster than an exponential ($\beta > 1$), indicating superdiffusive dynamics, with the exponent β decreasing monotonically with increasing q (Fig. 4d). Such q-dependent, superdiffusive dynamics were reported for fully arrested colloidal gels.[37] These measurements show that superdiffusive ballistic dynamics also occur during the formation and coarsening of gels undergoing spinodal decomposition *en route* to the arrested state. One may wonder whether these superdiffusive dynamics may arise from sedimentation of the large, coarsening domains. Previous studies on colloidal fluids undergoing spinodal decomposition[24,63] found that sedimentation effects become important once the domain size reaches a threshold value $L_c^* = 2\pi\Lambda_{cap}$, where Λ_{cap} is the capillary length defined by $\Lambda_{cap} = \sqrt{\gamma_{eff}/g\Delta\rho}$, where γ_{eff} is an effective interfacial tension defined by $\gamma_{eff} = \varepsilon\phi/\sigma^2$. Using these relationships, we find for our system $L_c^* \sim 180$ μm, which is a full order of magnitude larger than the largest domain sizes observed in our experiments. Therefore, we assume that sedimentation effects contribute negligibly to the observed microdynamics.

Both the appearance of these two dynamical modes as well as the q-dependence of the compressed exponent β are qualitatively the same for all of the age times studied, although the rates of both the diffusive and ballistic modes (proportional to $1/\tau_1$ and $1/\tau_2$, respectively) slow by approximately a factor of 4 over the extent of the linear coarsening regime. For longer age times, where the coarsening begins to slow and eventually arrest, DDM fails to provide reliable results since the superdiffusive dynamics slow to the point where an upper bound on $S(q,\tau)$ is missing, preventing reliable determination of the static parameters $A(q)$ and B.

The microscopic picture responsible for the two dynamical modes is clearly suggested by our combined DDM and TAM measurements. Specifically, we note that, at low q-values corresponding to $qL_c/2\pi < 1$ (i.e. at length scales larger than the domain size), the compressed exponent of the slow mode asymptotes to $\beta \sim 2$, corresponding to strictly ballistic motion, and decays to $\beta \sim 1$ with increasing q beyond this limit. From this, we hypothesize that the dynamics of spinodal decomposition can be explained by a combination of thermally-activated, collective fluctuations of fractal particle clusters within the droplet-rich domains (the fast relaxation process), which is convoluted with spatial or temporally heterogeneous ballistic motion of the domains themselves, most likely due to interfacial coarsening (the slow relaxation process).[2]

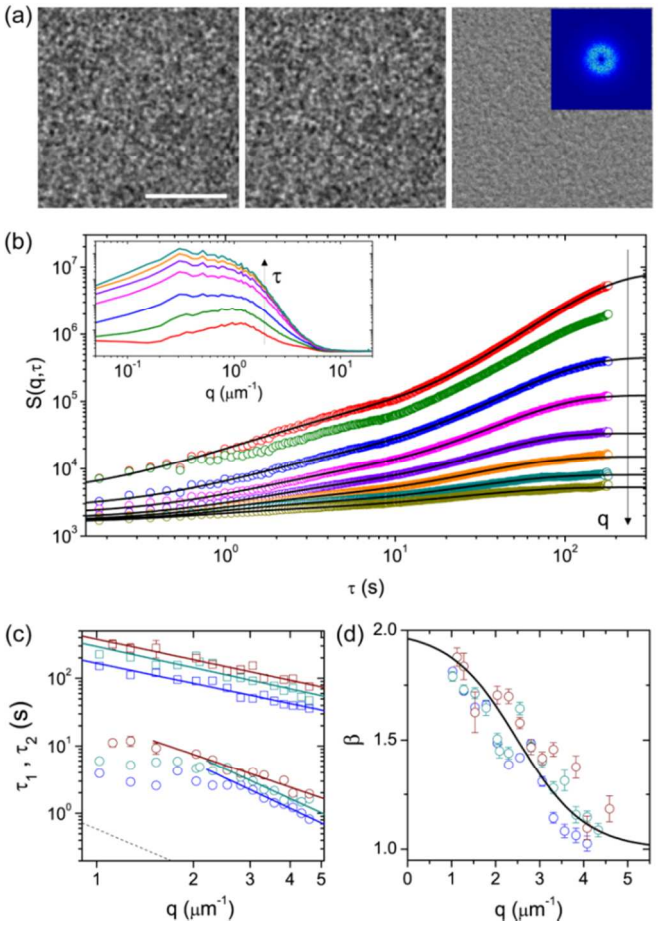

Fig. 4 Anomalous coarsening dynamics probed by DDM. (a) (Left to right) images taken at 240 and 244.5 s, difference image and its 2D FFT power spectrum (inset)**.** Scale bar is 50 μm. (b) $S(q,\tau)$ as a function of q (inset) and lag time (main figure). Black lines are fits to the experimental data according to eq. (3). From top to bottom, q = 1.019, 1.529, 2.038, 2.548, 3.057, 3.567, 4.076, 4.586 μm^{-1}. Inset: τ from bottom to top are 0.9, 4.5, 18, 54, 90, 125.5, 162.7 s. (c) q-dependent relaxation times of the fast (circles) and slow (squares) modes at aging times of 4 (blue), 7 (cyan) and 10 (brown) minutes. Lines are power-law fits to the data, with slopes (top to bottom) of -2.2 ± 0.3, -2.2 ± 0.5 and -1.6 ± 0.4 for $<\tau_1>$ and -1.0 ± 0.1, -1.0 ± 0.2, and -1.0 ± 0.2 for $<\tau_2>$. Dotted line indicates the diffusive relaxation time of dilute droplets. (d) q-dependence of the compressed exponent, β, with increasing q at t_{age} = 4 (blue), 7 (cyan) and 10 minutes (brown). Line is drawn to guide the eye.

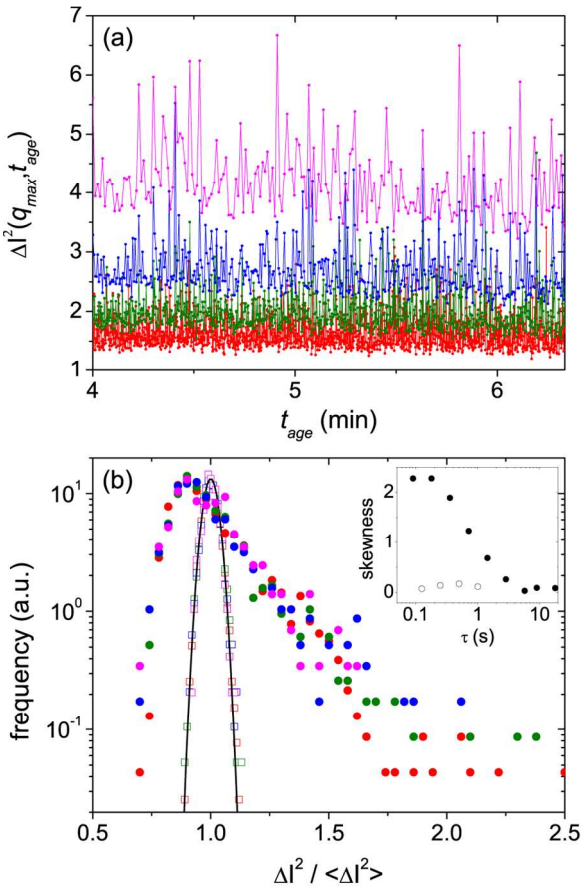

Fig. 5 Intermittent dynamics probed by fluctuations of $\Delta\bar{I}^2$. (a) $\Delta\bar{I}^2(q_{max})$ at τ = 0.09 (red), 0.18 (green), 0.36 (blue) and 0.72 s (magenta) as a function of aging time. (b) Normalized distribution of $\Delta\bar{I}^2$ for gelling nanoemulsions (closed symbols) and a dilute nanoparticle suspension (open symbols). Solid line indicates Gaussian behavior. Inset: skewness of the distributions in (b).

It was previously shown[37] that q-dependence of the scaling exponent β could be predicted by considering a dynamical process which acts intermittently within the fluid. To check for such intermittent behavior, we examine the FFT power fluctuation $\Delta\bar{I}(q,\tau,t_{age})^2$, which is the instantaneous value of $S(q,\tau)$ before performing the ensemble average. This quantity is equivalent to what has been used to study intermittent dynamics based on multi-speckle scattering techniques.[37] Specifically, we examine the fluctuations of $\Delta\bar{I}^2$ at $q = q_{max}(t_{age})$, which corresponds to the characteristic wavelength of the phase separating domains, at several different lag times τ (Fig. 5a). We find that the intensity fluctuations exhibit occasional excursions to higher values, corresponding to intermittent decreases in structural correlation for short time periods, similar to what is observed in a fully arrested colloidal gel.[37]

To further probe these intermittent dynamics, we examine the distributions of $\Delta\bar{I}^2$ about its mean value, $<\Delta\bar{I}^2>$ (Fig. 5b). For comparison, we also plot results for a dilute nanoparticle suspension (polystyrene beads of a = 95±6 nm at 2.6 wt% in water), which exhibits a Gaussian distribution as expected for an ergodic system driven by diffusive motion. By contrast, the distributions observed for the phase separating nanoemulsion deviates strongly from a Gaussian. To quantify the non-Gaussian behavior, we calculated the skewness of the distribution,[70] given by $s = <(\Delta\bar{I}^2-<\Delta\bar{I}^2>)^3>/(<(\Delta\bar{I}^2-<\Delta\bar{I}^2>)^2>)^{3/2}$ (Fig. 5b, inset and Fig. S7). The large skewness for the phase separating system further suggests the presence of intermittent dynamics which temporarily decrease correlations at short times. Although intermittent anomalous dynamics have been observed previously in fully arrested colloidal gels,[37] we have shown here that they also arise during coarsening *en route* to arrest, i.e. during spinodal decomposition.

Since the intermittent dynamics are observed on a length scale corresponding to $L_c = 2\pi/q_{max}$, we hypothesize that this slow mode is due to slow, directed motion of individual domains. To test this, we quantify the motion of individual textural features (i.e., the dense domains) identified by TAM. Specifically, we apply the particle tracking algorithms of Crocker and Grier[45,71] to the TAM correlation maps (Fig. 3a, lower row) to localize the centroids of features and track their motion with time (Fig. 6a, Video S2). We previously showed that this method provides superior feature localization for low-signal or otherwise corrupted images.[45] Overlaid on top of the correlation map are the initial and final positions of the identified centroids (cyan and red dots, respectively), and their full trajectories (blue lines). We stress that these trajectories represent collective motions of a large number of particles comprising individual dense domains, and not individual motions of single particles. This analysis therefore assumes that the centroid motion at this length scale is dominated by net motion of domains rather than exchange of particles between domains. It is clear that most trajectories are highly anisotropic, which suggests that the droplet-rich domains undergo directional motion, in agreement with the low-q dynamics observed by DDM. We note, however, that these directional trajectories still exhibit some fluctuations, which we hypothesize is due to the fast fluctuations within the domains. Thus, tracking the structural dynamics as described provides an independent confirmation of the hypothesized mechanism of microdynamics gleaned from DDM measurements.

The average microdynamics of the phase separated structure can be quantified by the mean squared displacement (MSD) of dense domains (Fig. 6b). The MSD exhibits diffusive motion (MSD ~ t) at short times due to thermal fluctuations and superdiffusive motion (MSD ~ $t^{1.35}$) at long times due to the directional motion of domains, further confirming the proposed microdynamics of coarsening. Specifically, we note that the transition between diffusive and superdiffusive motion occurs at observation times where t ~ τ_1, the relaxation time of the fast dynamics, which we attribute to overdamped fluctuations within domains. In this regard, the driving force for "diffusion" of domains is not the Brownian diffusion of individual particles, but rather the internal rearrangements of the gel network. One may wonder why an asymptotic exponent for the superdiffusive dynamics of 1.35 is observed, rather than the value of 2 expected for q→0 from DDM. The reason for this is the limited range of MSDs sampled by domains before coalescing, such that the long-time limit (which would correspond to q→0) is not sampled. We note that, if sample averaging is limited to domains with MSD ≈ L_c^2, the long-time exponent approaches the expected value of 2 (Fig. S8).

Tracking the directional motion of dense domains also elucidates newly observed collective dynamics that occur during spinodal decomposition prior to arrest (Fig. 6a). We highlight three dominant collective modes: a compressive mode where domains move towards each other to form larger domains (green boxes), an expansive mode where domains move away from each other to open up larger voids (cyan boxes), and a translational mode where domains move collectively in one direction (red boxes). We also observe that

the former two modes are often spatially correlated (overlaps of green and cyan boxes), and so are likely due to interfacially-driven coalescence of domains. The source of the translational mode is unclear. However, it could be due to large scale rearrangements brought about by relaxation of stresses built up within the elastic colloidal network during coarsening, similar to what has been proposed for viscoelastic phase separation.[3] In the end, this mode may well be the "microcollapse" events proposed by Bouchaud and co-workers,[41] but we stress that it is only one of several different collective modes occurring *en route* to arrest. Traditional two-point correlation functions fail to show distinct evidence of these collective modes (Fig. S9), and so we leave detailed analysis to future studies.

To further show that the compression and expansion modes are indeed due to coalescence, we track the rate of coalescence of domains (Fig. 6c), quantified by determining the number of domains disappearing from the tracked trajectories over time. The resulting number coalescence rate, r_c, decreases rapidly at short age times, and continues to decay more slowly at longer age times (Fig. 6c, left axis). However, we find that the rate of consumption of surface area (proportional to $r_c(t)L_c(t)^2$) is nearly constant in time (Fig. 6c, right axis). This suggests that, for this system, the coarsening of dense aggregated domains proceeds by an interfacially-limited coalescence process with nearly zero order kinetics. These kinetics could result from the short-time internal fluctuations at the interface between the colloid-rich and colloid-poor domains, which were apparent in recent confocal microscopy measurements on moderate-range attractive systems,[25] as well as in simulations of coarsening gels.[72] As shown above, these short-time fluctuations appear to be insensitive to larger-scale motion, and may provide the ultimate driving force for coarsening.

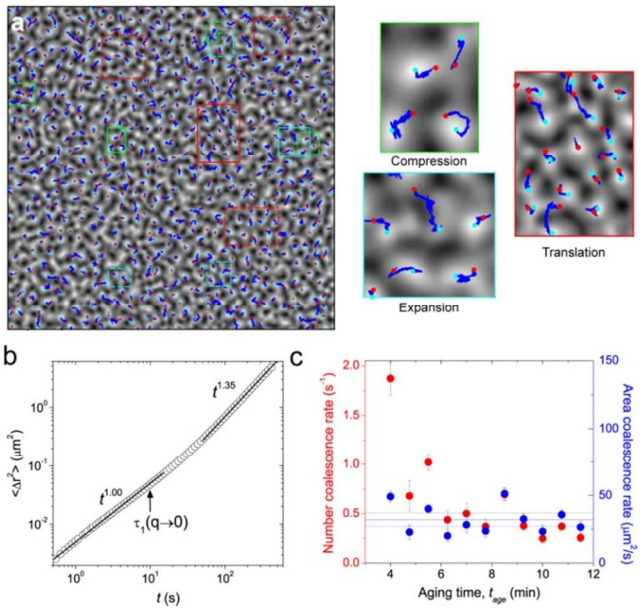

Fig. 6 Tracking local dynamics and collective modes of colloid-rich domains. (a) Motion of domains in real space**.** Trajectories of domains (blue lines) are overlaid on top of the starting correlation map, with cyan and red dots indicating the start and end points of trajectories, respectively. Three modes of collective motion are highlighted, including compressive (green boxes), expansive (cyan boxes) and translational (red boxes). Enlarged views of reprehensive regions from each mode are shown for clarity. (b) The mean squared displacement of all trajectories for t_{age} = 4 min, which becomes superdiffusive at long times. (c) The number (left axis) and area (right axis) rates of coalescence with increasing aging time. The area coalescence rate is approximately constant (32.2±4.4 μm²/s) within the imaging area.

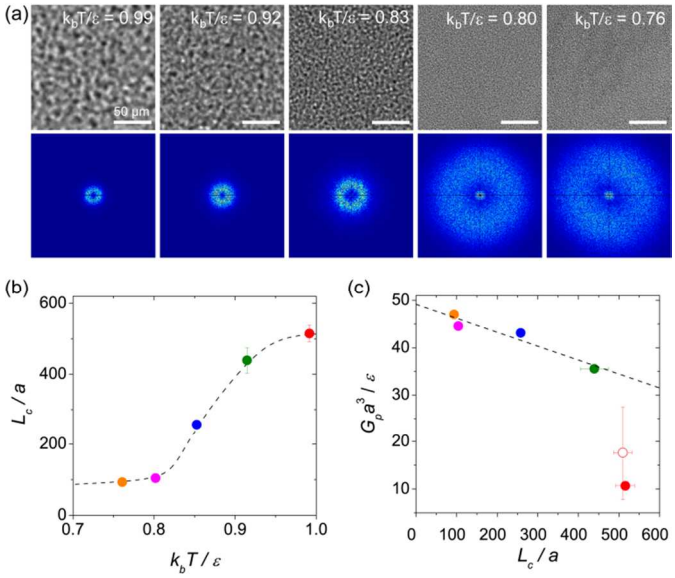

Fig. 7 Effect of thermal quench depth on arrested structure and rheology. (a) Bright field images (top) and corresponding Fourier transforms (bottom) of nanoemulsion gels arrested at different quench depths. (b) Characteristic length scales (L_c) extracted from the peak positions in panel a. (c) Normalized elastic moduli as a function of the characteristic length scales. Open symbol represents replicate measurements of the sample at the shallowest quench (red point). Dotted lines are drawn to guide the eye.

3.3 Quench-dependence of the arrested state

To this point, we have only reported results for a gel experiencing a quasi-equilibrium quench to the initial point of observable phase instability. To further study the quench-dependence of spinodal decomposition, we explored the dependence of the arrested microstructure of our nanoemulsion colloidal gels on the depth of the temperature quench into the spinodal region, as well as its relation to the rheological properties of the resulting gels upon arrest. To do so, we first equilibrated samples at room temperature ($T << T_{gel}$), and then quickly heated them to desired temperatures where $T > T_{gel}$ to achieve a fast quench to a relative depth below the spinodal, k_bT/ε (Fig. 1). Optical images of samples after the structure becomes arrested (Figure 7a, top row) clearly show that the gel structure arrests at smaller length scales with deeper quenches. Similar behavior has been observed in gelation of colloid-polymer mixtures,[12,15,22] globular protein solutions[73] and were suggested by computer simulation.[26] The FFT of images of the arrested structure exhibit a clear ring (Fig. 7a, bottom row), which corresponds to a peak in the radially-averaged intensity. The extracted values of L_c (Fig. 7c) decrease systematically by an order of magnitude for k_bT/ε ~ 1.0-0.76. Interestingly, L_c becomes nearly quench-independent for sufficiently deep quenches ($k_bT/\varepsilon < 0.8$).

Meanwhile, we performed rheological measurements on these samples at similar conditions: samples are equilibrated at 20 °C on the rheometer, after which we quickly ramp temperature to the desired quench, k_bT/ε. The linear viscoelastic moduli were then monitored until time-invariant behavior was obtained (Fig. S3.2). The final arrested plateau value of the elastic modulus, G_p, increases dramatically with increasing quench depth by nearly an order of magnitude. This corresponds to a systematic decrease of the gel modulus with increasing L_c, even though previous neutron scattering measurements showed that the internal fractal microstructure of the dense domains remains insensitive to quench depth.[42] This

is captured in Fig. 7d, where the reduced modulus $G_p a^3/\varepsilon$, is plotted versus the dimensionless correlation length (L_c/a) of phase separation. For small values of L_c/a (deep quenches), the modulus decreases linearly with increasing L_c/a. Interestingly, this scaling is precisely what was anticipated by recent simulations of coarsening in suspensions with moderate-range attraction,[72] and has also been predicted for the cluster-size dependence of colloidal gels that form by percolation in the homogeneous fluid phase.[74] For larger values of L_c (i.e. quenches of $k_bT/\varepsilon \sim 1.0$), the experimentally measured moduli become highly irreproducible, and often fall considerably below this scaling (Fig. 7c, red symbols).

Thus, the elasticity of colloidal gels depend significantly on the length scale of arrested spatial heterogeneity in the density of particle clusters, here brought about by SD. Although this is perhaps expected, it highlights how the rheology of colloidal gels depends dramatically on the large-scale structural heterogeneity of the fluid, in addition to the known impact of the local-scale distribution and rigidity of particle "bonds" in the elastic network.[32,75] In this case, the viscoelasticity may be rationalized as emerging from a percolated network of colloid-rich "blobs" comprising the dense domains brought about by SD, regardless of the specific internal structure within them. Our results both confirm recent hypotheses from simulations for sufficiently deep quenches,[72,74] and call for more thorough investigations of the catastrophic decrease in elasticity observed sufficiently close to the spinodal.

4 Conclusions

We have demonstrated arrested spinodal decomposition as the mechanism of gelation in a thermoreversible colloidal system with moderate-range attractions at volume fractions above ϕ_c. This finding generalizes the phenomena found in earlier studies on other polymer-colloid mixtures.[14,22,23,25] Our results stand in contrast to other studies of thermoreversible colloids with near-contact attractions,[27] and highlight the range of the attractive potential as a significant determining factor in the mechanism of gelation, as suggested by theory.[76]

New imaging tools (TAM and DDM) are effective probes of the microdynamics driving coarsening at large, previously unstudied length scales, which exhibit characteristics of interfacially-dominated SD before finally coming to arrest. The q-dependent dynamics exhibit a combination of fast diffusive dynamics and slow, intermittent superdiffusive dynamics, the latter of which is ballistic at length scales above L_c. We rationalize these dynamics as arising from thermal fluctuations of particle clusters within the colloid-rich domains, and slow but persistent directional motion of individual domains driven by interfacial coarsening, respectively.

Our studies identify new collective modes, including coalescence and collective translation of domains, reminiscent of the phenomenological processes proposed explain the dynamics previously observed in fully arrested gels.[37,41] These collective modes warrant further inquiry, and may provide a more thorough understanding of the processes leading to arrest of SD, as well as aging after kinetic arrest occurs. More broadly, similar techniques could be employed to give insight into the anomalous dynamics of other systems, including colloidal glasses exhibiting a combination of fast diffusive and slow sub-diffusive relaxation modes.[77]

The quench depth at which SD is initiated provides an effective means to control the arrested structure and rheology of colloidal gels, which in this case can be thought of as a network of dense domains, whose viscoelasticity depends linearly on the arrested length scale of phase separation. We anticipate this to have great potential in templating materials with controllable porosity as a potential alternative to "bijels",[78] since the quench depth provides facile control of the arrested structure without changing the composition of the system. Ongoing studies are aimed at probing the dependence of the coarsening dynamics and arrest on a number of other variables important to the system, including volume fraction and the range of interparticle attraction, as well as the rate at which the system is quenched, in order to test their generality in the nanoemulsion system. Ultimately, we hope that our results can serve as a benchmark for developing future theoretical models to describe coarsening, spinodal decomposition, and arrested states in attractive colloidal fluids.

Acknowledgements

Y. Gao was supported in part by the MRSEC Program of the National Science Foundation under Award No. DMR 1121053, and J. Kim was supported by the National Science Foundation under Award No. CBET 1351371.

Notes and references

[a] Department of Chemical Engineering, University of California Santa Barbara, Santa Barbara CA 93105-5080.

[b] Current address: Department of Chemistry, Physical and Theoretical Chemistry Laboratory, University of Oxford, South Parks Road, Oxford, OX1 3QZ, UK

[*] Address correspondence to helgeson@engineering.ucsb.edu.

†Electronic Supplementary Information (ESI) available: Summary of previous microdynamics measurements, time sweep rheological measurements, TAM and DDM validation, supplementary DDM and particle tracking data, videos of spinodal coarsening used in this work. See DOI: 10.1039/b000000x/

1. S. Puri, *Phase Transitions*, 2004, **77**, 407-431.
2. E. D. Siggia, *Physical review A*, 1979, **20**, 595.
3. H. Tanaka, *Journal of Physics: Condensed Matter*, 2000, **12**, R207.
4. J. Erlebacher, M. J. Aziz, A. Karma, N. Dimitrov and K. Sieradzki, *Nature*, 2001, **410**, 450-453.
5. L. Li, X. Shen, S. W. Hong, R. C. Hayward and T. P. Russell, *Angewandte Chemie International Edition*, 2012, **51**, 4089-4094.
6. B. Dong, T. Zhan, X. Liu, L. Jiang, F. Liu, X. Hu and J. Zi, *Physical Review E*, 2011, **84**, 011915.
7. E. R. Dufresne, H. Noh, V. Saranathan, S. G. Mochrie, H. Cao and R. O. Prum, *Soft Matter*, 2009, **5**, 1792-1795.
8. E. Herzig, K. White, A. Schofield, W. Poon and P. Clegg, *Nature materials*, 2007, **6**, 966-971.
9. E. Zaccarelli, *Journal of Physics: Condensed Matter*, 2007, **19**, 323101.
10. H. Verduin and J. K. Dhont, *Journal of colloid and interface science*, 1995, **172**, 425-437.
11. W. Poon, A. Pirie, M. Haw and P. Pusey, *Physica A: Statistical Mechanics and its Applications*, 1997, **235**, 110-119.

12. S. Manley, H. Wyss, K. Miyazaki, J. Conrad, V. Trappe, L. Kaufman, D. Reichman and D. Weitz, *Physical review letters*, 2005, **95**, 238302.

13. F. Cardinaux, T. Gibaud, A. Stradner and P. Schurtenberger, *Physical review letters*, 2007, **99**, 118301.

14. P. J. Lu, E. Zaccarelli, F. Ciulla, A. B. Schofield, F. Sciortino and D. A. Weitz, *Nature*, 2008, **453**, 499-503.

15. E. Zaccarelli, P. J. Lu, F. Ciulla, D. A. Weitz and F. Sciortino, *Journal of Physics: Condensed Matter*, 2008, **20**, 494242.

16. G. Foffi, C. De Michele, F. Sciortino and P. Tartaglia, *The Journal of chemical physics*, 2005, **122**, 224903.

17. J. C. F. Toledano, F. Sciortino and E. Zaccarelli, *Soft Matter*, 2009, **5**, 2390-2398.

18. E. Del Gado, A. Fierro, L. de Arcangelis and A. Coniglio, *Physical Review E*, 2004, **69**, 051103.

19. M. A. Miller and D. Frenkel, *The Journal of chemical physics*, 2004, **121**, 535-545.

20. M. G. Noro and D. Frenkel, *The Journal of chemical physics*, 2000, **113**, 2941-2944.

21. D. Fu, Y. Li and J. Wu, *Physical Review E*, 2003, **68**, 011403.

22. J. Conrad, H. Wyss, V. Trappe, S. Manley, K. Miyazaki, L. Kaufman, A. Schofield, D. Reichman and D. Weitz, *Journal of Rheology (1978-present)*, 2010, **54**, 421-438.

23. A. Bailey, W. Poon, R. J. Christianson, A. Schofield, U. Gasser, V. Prasad, S. Manley, P. Segre, L. Cipelletti, W. Meyer, M. Doherty, A. Sankaran, A. Jankovsky, W. Shiley, J. Bowen, J. Eggers, C. Kurta, T. Lorik, P. Pusey and D. Weitz, *Physical review letters*, 2007, **99**, 205701.

24. L. J. Teece, M. A. Faers and P. Bartlett, *Soft Matter*, 2011, **7**, 1341-1351.

25. I. Zhang, C. P. Royall, M. A. Faers and P. Bartlett, *Soft Matter*, 2013, **9**, 2076-2084.

26. V. Testard, L. Berthier and W. Kob, *Physical review letters*, 2011, **106**, 125702.

27. A. P. Eberle, N. J. Wagner and R. Castañeda-Priego, *Physical review letters*, 2011, **106**, 105704.

28. M. Filali, M. J. Ouazzani, E. Michel, R. Aznar, G. Porte and J. Appell, *The Journal of Physical Chemistry B*, 2001, **105**, 10528-10535.

29. F. Molino, J. Appell, M. Filali, E. Michel, G. Porte, S. Mora and E. Sunyer, *Journal of Physics: Condensed Matter*, 2000, **12**, A491.

30. G. Porte, C. Ligoure, J. Appell and R. Aznar, *Journal of Statistical Mechanics: Theory and Experiment*, 2006, **2006**, P05005.

31. B. Chung, S. Ramakrishnan, R. Bandyopadhyay, D. Liang, C. Zukoski, J. Harden and R. Leheny, *Physical review letters*, 2006, **96**, 228301.

32. C. J. Dibble, M. Kogan and M. J. Solomon, *Physical Review E*, 2006, **74**, 041403.

33. Y. Gao and M. Kilfoil, *Physical review letters*, 2007, **99**, 078301.

34. A. Madsen, R. L. Leheny, H. Guo, M. Sprung and O. Czakkel, *New Journal of Physics*, 2010, **12**, 055001.

35. C. P. Royall, S. R. Williams, T. Ohtsuka and H. Tanaka, *Nature materials*, 2008, **7**, 556-561.

36. L. Cipelletti, S. Manley, R. Ball and D. Weitz, *Physical review letters*, 2000, **84**, 2275.

37. A. Duri and L. Cipelletti, *EPL (Europhysics Letters)*, 2006, **76**, 972.

38. H. Guo, S. Ramakrishnan, J. L. Harden and R. L. Leheny, *The Journal of chemical physics*, 2011, **135**, 154903.

39. E. Del Gado and W. Kob, *Physical review letters*, 2007, **98**, 028303.

40. M.-A. Suarez, N. Kern, E. Pitard and W. Kob, *The Journal of chemical physics*, 2009, **130**, 194904.

41. J.-P. Bouchaud and E. Pitard, *The European Physical Journal E*, 2001, **6**, 231-236.

42. M. E. Helgeson, Y. Gao, S. E. Moran, J. Lee, M. Godfrin, A. Tripathi, A. Bose and P. S. Doyle, *Soft Matter*, 2014, **10**, 3122-3133.

43. M. E. Helgeson, S. E. Moran, H. Z. An and P. S. Doyle, *Nature materials*, 2012, **11**, 344-352.

44. J. Kim, Y. Gao, C. Hebebrand, E. Peirtsegaele and M. E. Helgeson, *Soft Matter*, 2013, **9**, 6897-6910.

45. Y. Gao and M. E. Helgeson, *Optics express*, 2014, **22**, 10046-10063.

46. R. Cerbino and V. Trappe, *Physical review letters*, 2008, **100**, 188102.

47. F. Giavazzi, D. Brogioli, V. Trappe, T. Bellini and R. Cerbino, *Physical Review E*, 2009, **80**, 031403.

48. M. H. Lee, F. L. Beyer and E. M. Furst, *Journal of colloid and interface science*, 2005, **288**, 114-123.

49. J. M. Kim, J. Fang, A. P. Eberle, R. Castañeda-Priego and N. J. Wagner, *Physical review letters*, 2013, **110**, 208302.

50. S. Netemeyer and E. D. Glandt, *The Journal of chemical physics*, 1986, **85**, 6054-6059.

51. F. Del Rio, E. Avalos, R. Espindola, L. F. Rull, G. Jackson and S. Lago, *Molecular Physics*, 2002, **100**, 2531-2546.

52. E. El Mendoub, J.-F. Wax, I. Charpentier and N. Jakse, *Molecular Physics*, 2008, **106**, 2667-2675.

53. M. E. Helgeson and N. J. Wagner, *The Journal of chemical physics*, 2011, **135**, 084901.

54. A. Zilman, J. Kieffer, F. Molino, G. Porte and S. Safran, *Physical review letters*, 2003, **91**, 015901.

55. J. Kim, D. Merger, M. Wilhelm and M. E. Helgeson, *Journal of Rheology (1978-present)*, 2014, **58**, 1359-1390.

56. A. Zaccone, J. J. Crassous, B. Béri and M. Ballauff, *Physical review letters*, 2011, **107**, 168303.

57. A. Zaccone, H. Winter, M. Siebenbürger and M. Ballauff, *Journal of Rheology (1978-present)*, 2014, **58**, 1219-1244.

58. S. Asakura and F. Oosawa, *Journal of Polymer Science*, 1958, **33**, 183-192.

59. A. Vrij, *Pure and Applied Chemistry*, 1976, **48**, 471-483.

60. H. H. Winter and F. Chambon, *Journal of Rheology (1978-present)*, 1986, **30**, 367-382.

61. L. Cipelletti and D. Weitz, *Review of Scientific Instruments*, 1999, **70**, 3214-3221.

62. H. Furukawa, *Physica A: Statistical Mechanics and its Applications*, 1983, **123**, 497-515.

63. D. Aarts, R. Dullens and H. Lekkerkerker, *New Journal of Physics*, 2005, **7**, 40.

64. P. J. Lu, F. Giavazzi, T. E. Angelini, E. Zaccarelli, F. Jargstorff, A. B. Schofield, J. N. Wilking, M. B. Romanowsky, D. A. Weitz and R. Cerbino, *Physical review letters*, 2012, **108**, 218103.

65. F. Ferri, A. D'Angelo, M. Lee, A. Lotti, M. Pigazzini, K. Singh and R. Cerbino, *The European Physical Journal-Special Topics*, 2011, **199**, 139-148.

66. K. He, M. Spannuth, J. C. Conrad and R. Krishnamoorti, *Soft Matter*, 2012, **8**, 11933-11938.

67. V. A. Martinez, R. Besseling, O. A. Croze, J. Tailleur, M. Reufer, J. Schwarz-Linek, L. G. Wilson, M. A. Bees and W. C. Poon, *Biophysical journal*, 2012, **103**, 1637-1647.

68. S. Buzzaccaro, M. D. Alaimo, E. Secchi and R. Piazza, *Journal of Physics: Condensed Matter*, 2015, **27**, 194120.

69. A. Krall and D. Weitz, *Physical review letters*, 1998, **80**, 778.

70. H. Bissig, S. Romer, L. Cipelletti, V. Trappe and P. Schurtenberger, *PhysChemComm*, 2003, **6**, 21-23.

71. J. C. Crocker and D. G. Grier, *Journal of colloid and interface science*, 1996, **179**, 298-310.

72. R. N. Zia, B. J. Landrum and W. B. Russel, *Journal of Rheology (1978-present)*, 2014, **58**, 1121-1157.

73. T. Gibaud and P. Schurtenberger, *Journal of Physics: Condensed Matter*, 2009, **21**, 322201.

74. A. Zaccone, H. Wu and E. Del Gado, *Physical review letters*, 2009, **103**, 208301.

75. J. P. Pantina and E. M. Furst, *Physical review letters*, 2005, **94**, 138301.

76. R. Jadrich and K. S. Schweizer, *The Journal of chemical physics*, 2011, **135**, 234902.

77. F. Augusto de Melo Marques, R. Angelini, E. Zaccarelli, B. Farago, B. Ruta, G. Ruocco and B. Ruzicka, *Soft Matter*, 2015, **11**, 466-471.

78. M. N. Lee and A. Mohraz, *Advanced Materials*, 2010, **22**, 4836-4841.